Detection of ground motions using high-rate GPS time-series

Author(s):
Psimoulis, Panos A.; Houlié, Nicolas (iD); Habboub, Mohammed; Michel, Clotaire (iD); Rothacher, Markus

Detection of ground motions using high-rate GPS time-series

Panos A. Psimoulis,[1] Nicolas Houlié,[2,3,4] Mohammed Habboub,[1] Clotaire Michel[4] and Markus Rothacher[2]

[1]*Nottingham Geospatial Institute, University of Nottingham, Nottingham NG7 2TU, UK. E-mail: panagiotis.psimoulis@nottingham.ac.uk*
[2]*Mathematical and Physical Geodesy (MPG), Institute of Geodesy and Photogrammetry, ETH Zurich, 8093 Zurich, Switzerland*
[3]*Seismology and Geodynamics (SEG), Institute of Geophysics, ETH Zurich, 8092 Zurich, Switzerland*
[4]*Swiss Seismological Service (SED), Institute of Geophysics, ETH Zurich, 8092 Zurich, Switzerland*

SUMMARY

Monitoring surface deformation in real-time helps at planning and protecting infrastructures and populations, manages sensitive production (i.e. SEVESO-type) and mitigates long-term consequences of modifications implemented. We present RT-SHAKE, an algorithm developed to detect ground motions associated with landslides, subsurface collapses, subsidences, earthquakes or rock falls. RT-SHAKE detects first transient changes in individual GPS time-series before investigating for spatial correlation(s) of observations made at neighbouring GPS sites and eventually issues a motion warning. In order to assess our algorithm on fast (seconds to minute), large (from 1 cm to metres) and spatially consistent surface motions, we use the 1 Hz GEONET GNSS network data of the Tohoku-Oki M_w9.0 2011 as a test scenario. We show that the delay of detection of seismic wave arrival by GPS records is of ∼10 s with respect to an identical analysis based on strong-motion data and this time delay depends on the level of the time-variable noise. Nevertheless, based on the analysis of the GPS network noise level and ground motion stochastic model, we show that RT-SHAKE can narrow the range of earthquake magnitude, by setting a lower threshold of detected earthquakes to M_w6.5–7, if associated with a real-time automatic earthquake location system.

Key words: Earthquake Early Warning; Satellite Geodesy; Strong ground motion; Seismic-wave propagation.

1 INTRODUCTION

Detecting and characterizing surface motion in real-time enable the protection of infrastructures and populations, manage sensitive production (i.e. SEVESO-type) and mitigate long-term consequences (Bertazzi *et al.* 1989; Ying *et al.* 2014; Ferreira & Karali 2015). Earthquakes, along with landslides, are the most challenging processes to monitor in real-time because (1) they unexpectedly develop in a very short lapse of time (from seconds to few minutes) and (2) the maximum displacement (from zero to several meters) is unknown until the end of the event. Other processes are either of smaller amplitudes and/or require longer periods to develop (e.g. volcanic inflation, geothermal activities, etc.; Fig. 1).

Nowadays earthquake early warning (EEW) systems enable to quantify magnitudes of earthquakes before the end of the rupture during ongoing seismic wave propagation (Allen & Kanamori 2003; Olson & Allen 2005; Lewis & Ben-Zion 2008; Allen *et al.* 2009; Edwards *et al.* 2010; Doi 2011; Espinosa-Aranda *et al.* 2011; Colombelli *et al.* 2013; Kawamoto *et al.* 2017; Psimoulis *et al.* 2018). Those systems required the installation of dense seismic network to minimize the detection delays and of geodetic systems to minimize the risk of magnitude underestimation. Likewise, geodetic systems, and mainly GPS networks (Michoud *et al.* 2013), have been developed as part of landslide warning system, for real-time landslides monitoring focusing on the detection of motion (Benoit *et al.* 2015; Lienhart 2015; Zhou *et al.* 2018) and its correlation with soil moisture, groundwater pressures and ground displacement, which could lead to landslide triggering (Kristensen & Blikra 2011; Wang *et al.* 2011). Furthermore, GPS records have been proved capable for the monitoring of short-period dynamic motion (Psimoulis *et al.* 2008; Moschas *et al.* 2014; Haberling *et al.* 2015), of the slow static ground deformation, associated with volcanic (Houlié *et al.* 2006; Trota *et al.* 2006; Newman *et al.* 2012; Tu *et al.* 2013), of geothermal activities (Fournier & Jolly 2014; Heimlich *et al.* 2015) and of seismological applications related to earthquake response activities (Bock *et al.* 2004; Ohta *et al.* 2006; Yokota *et al.* 2009; Newman *et al.* 2012; Wright *et al.* 2012; Larson 2013; Melgar *et al.* 2013; Kelevitz *et al.* 2017; Michel *et al.* 2017).

Until now, however, the potential of GNSS process in real-time using the Precise Point Positioning (PPP) mode (Ge *et al.* 2008; Jokinen *et al.* 2013) complements already existing EEW system based on seismic data only (Blewitt *et al.* 2009; Crowell *et al.* 2009;
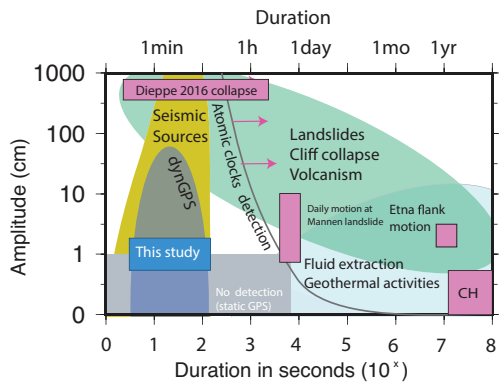
Figure 1. Amplitude versus duration diagram for various geological catastrophic processes. We show detection limits for GPS, dynamic GPS and microgravimetry. In this study, as in any real-time algorithm, we focus on detecting small amplitudes as fast as possible. dynGPS curves are from analyses of dynamic GPS time-series recorded during seismic wave propagations (Houlié *et al.* 2011, 2014; Kelevitz *et al.* 2017). Sensitivity curve for atomic clock are from Bondarescu *et al.* (2012, 2015). Slower deformation cases are from Houlié *et al.* (2006) for Etna and Houlié *et al.* (2018) for deformation in Switzerland (indicated by CH in the figure). Static GPS is able to detect motion larger than 1 cm for duration larger than 10^{-4} s and then is naturally well supplemented by the Blum's silica inclinometer (Blum *et al.* 1959; Saleh *et al.* 1991; Llubes *et al.* 2008).

Plag *et al.* 2012; Geng *et al.* 2013a). It has been demonstrated that a warning could have been issued ∼20 s after the seismic network detection, proving the potential of GPS in that field (Allen & Ziv 2011; Colombelli *et al.* 2013). In these studies, GPS networks are being used to provide the amplitude of the displacement, without though functioning in an autonomous triggering mode but being dependent on other monitoring sensors (i.e. seismometers, etc.) of the early warning systems.

In this study, we take advantage of relative high density (one site every 30–50 km and a rupture length of ∼700 km) of the GEONET-Japan GPS networks in order to detect, in real-time or near real-time, and constrain the magnitude of (i) very large events ($M_w 8 +$) and (ii) slow event processes of moderate initial displacement but large final displacement (i.e. up to m; landslides, geothermal activity). The method RT-SHAKE, which is presented, was developed based on pre-existing algorithm, which is commonly applied for the detection of seismic signal using of seismograms (Allen 1978) or GPS records (Allen & Ziv 2011; Colombelli *et al.* 2013). RT-SHAKE was tuned (1) to be compatible with GPS data characteristics (i.e. noise, sampling rate), (2) to mitigate the impact of GPS errors and outliers on the detection process and (3) to provide a reliable and robust detection of the ground motion over multiple orders of displacement and time magnitudes. RT-SHAKE is then designed to enhance the sensitivity and robustness of the GPS network data in early warning applications, with respect to existing algorithms (Allen & Ziv 2011; Colombelli *et al.* 2013) for GPS data, and to supplement the existing more sensitive seismic sensor networks.

A potential autonomous application of GNSS network for early warning system would not aim to replace the existing seismic sensor networks, but (i) to enhance the density of the monitoring stations, for areas where the seismic networks are not dense, improving consequently the overall performance of early warning systems, (ii) to supplement the seismic sensors for potential malfunction due to their weaknesses (i.e. clipping, tilting; Geng *et al.* 2013b) and (iii) to develop more prompt and independent procedures for the estimation of earthquake characteristics, which are using seismogeodetic data

by integrating GPS and seismic data (Bock *et al.* 2011; Tu *et al.* 2013; Melgar *et al.* 2013; Geng *et al.* 2013a,b) or even only GPS displacement waveforms (Crowell *et al.* 2009; Colombelli *et al.* 2013).

To validate RT-SHAKE solutions, we used a GPS data set collected during the Tohoku-Oki $M_w 9.0$ 2011 event, which was selected for the following reasons. First, this case study satisfied the conditions of (i) long duration of development, as the seismic rupture lasted ∼300 s (i.e. slow process) and (ii) large maximum ground displacement, with the largest coseismic motions reaching up to 4 m (i.e. large event), but could have been still detected by real-time GPS network (RTK mode) as soon as the displacement exceeded ∼1 cm (i.e. GPS data noise level). Second, the two above-mentioned conditions and the characteristic step-waveform displacement of the GPS sites close to the epicentre represent not only the main characteristics of large earthquakes (Colombelli *et al.* 2013) but also of landslides' ground motion patterns (Wang 2012; Benoit *et al.* 2015). Third, the examined case study should reflect the efficiency in detecting seismic motion larger than the GPS data noise level (i.e. >1 cm); motions corresponding to large ($M > 7$; Larson *et al.* 2003; Bock *et al.* 2004; Allen & Ziv 2011; Colombelli *et al.* 2013) or even moderate earthquakes (e.g. L'Aquila $M_w 6.3$ 2009; Cirella *et al.* 2009; Avallone *et al.* 2011).

In addition to first goals, the complex seismic wave propagation of the Tohoku-Oki $M_w 9.0$ 2011 event, due to the multipatch rupture (Koketsu *et al.* 2011; Suzuki *et al.* 2011; Psimoulis *et al.* 2014), and the broad GPS network (i.e. up to 800 km from the epicentre) allows to evaluate the performance of the developed method in detecting complex and broad range of ground motion waveforms and amplitude, varying across the GPS network from m-level amplitude (close to the epicentre) to a few cm-level amplitude (far from the epicentre), due to the seismic motion attenuation.

Finally, for the Tohoku-Oki $M_w 9.0$ event it was possible to use GPS data in post-processing mode, simulate real-time data and evaluate its accuracy, reliability and consistency by comparing against available RTK solutions of GPS network data (Wright *et al.* 2012) and two existing strong-motion sensors systems. We show that the detection of the seismic signal by the GPS records is generally in agreement with that by the strong-motion records, with a time delay of ∼10 s, but faster than the GPS detection of algorithms of previous studies (see Colombelli *et al.* 2013).

2 METHODOLOGY

Detection algorithms using of seismic data are focusing on the detection of the arrival of the *P*-waves (Allen 1978), the wave propagating the fastest through the Earth. Because of the dispersive character of the seismic waves, destructive waves (i.e. *S*-waves) arrive after a delay that can be exploited to alert of the approach of potentially damaging waves. Therefore, hopes to dispatch an alert is best in the far field of seismometer.

The detection of *P*-wave is completed when a change of the low-frequency noise of the seismometer is detected. The noise of the seismic records is minimized by applying successively (1) a band-pass filter and (2) a short-term data average versus long-term data average trigger algorithm (Allen 1978), broadly known as STA/LTA algorithm. The long- and short-term data averages correspond to the low-frequency noise and the high-frequency seismic signal of the seismic waves, respectively. The short-term and long-term time windows of the averages may vary, with the values of 1 and 10 s, respectively, considered as indicative. Based on the corresponding
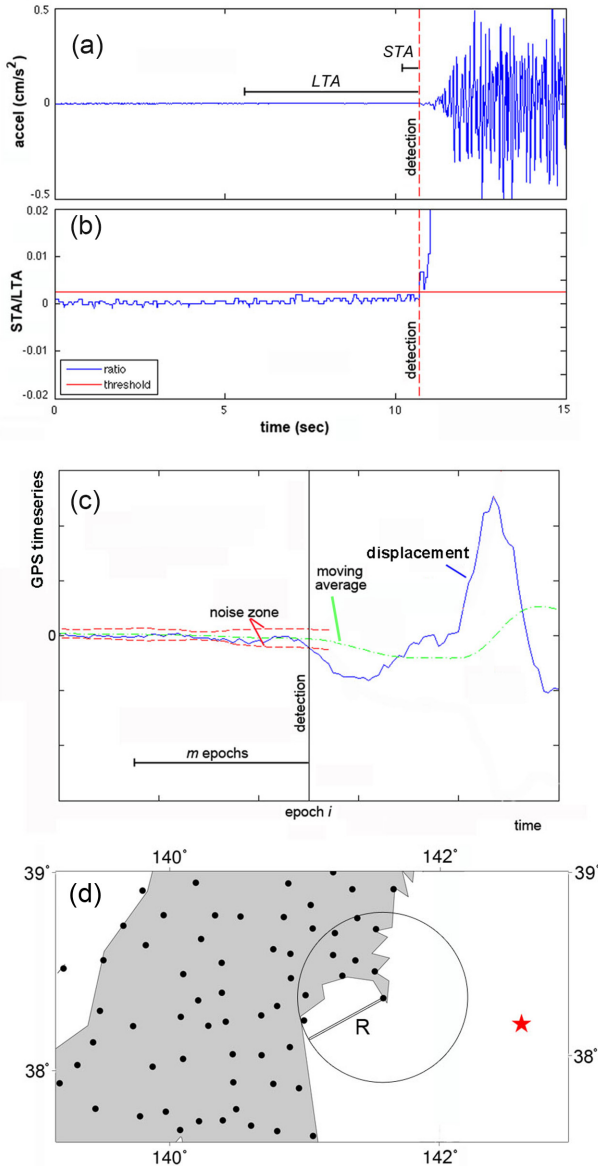
Figure 2. (a) The first 15 s of the acceleration record of MYG011 strong-motion site for the $M_w 9.0$ Tohoku 2011 earthquake and (b) the computed corresponding STA/LTA ratio with the threshold for the detection of first seismic wave arrival. (c) The detection of seismic signal in GPS networks, where first the seismic signal is detected based on the noise level of GPS time-series and (d) then a check is made for detection of consistent signal in neighbouring stations in distance R from the detected site. The red star expressed the earthquake epicentre.

computed averages derives the STA/LTA ratio, which is examined whether it is larger than a specific threshold (e.g. an indicative value of the threshold is 3). In case of the STA/LTA ratio to be larger than the threshold, it means that the incoming waveforms have been disturbed, and the characteristics of the disturbed waveforms define then the triggering parameters (Figs 2a and b).

The tuning of threshold is crucial to avoid false detection of seismic signal (i.e. due to GPS noise cycle slips, outliers, etc.; Kawamoto *et al.* 2017). In one of the first studies for application of GPS networks in early warning systems, Crowell *et al.* (2009) used an *a priori* threshold (i.e. 0.1 m total displacement), which was 5–10 times larger than the precision of GPS data (i.e. ∼1 cm;

Genrich & Bock 2006), to detect the arrival time at each GPS site and estimate the corresponding total displacement. However, the conservative threshold was one of the reasons for biased estimation of earthquake parameters (Crowell *et al.* 2009). In more recent studies, the STA/LTA approach was applied to GPS network data for the accurate detection of the arrival of the ground motion at each GPS station and determination of the coseismic displacement, which was then used to estimate earthquake magnitude (Allen & Ziv 2011; Ohta *et al.* 2012; Colombelli *et al.* 2013; Kawamoto *et al.* 2016). To avoid false detection of seismic signal in GPS time-series, Allen & Ziv (2011) defined the STA/LTA threshold to be larger than 10, while Ohta *et al.* (2012) used a lower threshold (e.g. 4), with higher *a priori* GPS noise level though. Even though all the above studies have proposed successful and reliable trigger techniques for GPS data, there is a delay in the detection of the seismic signal in the GPS data, mainly due to the relatively high thresholds criteria (e.g. 28 s delay for the Tohoku-Oki 2011 case study in Colombelli *et al.* 2013).

RT-SHAKE is based on a processing strategy that is similar to the STA/LTA, coupled by a spatial data analysis, which aims to detect seismic motion more sensitively and robustly. More specifically, contrary to other existing detection algorithms (Allen & Ziv 2011; Ohta *et al.* 2012), once RT-SHAKE detects a seismic signal, it assesses the reliability of the detected seismic signal by checking for detections of consistent seismic signal at surrounding stations in a short time interval. The spatial check is used to eliminate the impact of site-specific GPS errors, such as outliers, multipath, cycle slips, etc., which could not be filtered by the STA/LTA algorithm but should not also characterize the GPS displacement time-series of surrounding stations (Ohta *et al.* 2012). The detection algorithm runs separately on all local reference frame components (east, north and up) at each GPS site in order to make more sensitive the procedure to the detection of small displacement which can appear initially only to one of the three components, depending on the seismic waves directivity and considering also the different noise level between the horizontal and the vertical components (Psimoulis *et al.* 2015). The algorithm is applied epoch by epoch, considering that the GPS records are sampled at 1 Hz.

At the epoch i of the displacement time-series u_i of the station q, we compute the mean average u_{mi} of the previous m data (i.e. from $i - m - 1$ to $i - 1$), as given by the expression (Supporting Information Fig. SA1)

$$u_{mi} = \frac{\sum_{i-m-1}^{i-1} u_i}{m} \tag{1}$$

and the standard error σ_i of the previous m data (i.e. from $i - m - 1$ to $i - 1$), defined as

$$\sigma_i = \sqrt{\frac{\sum_{i-m-1}^{i-1} (u_i - u_{mi})^2}{(m - 1)}}. \tag{2}$$

Generally, the trend of the moving mean average of a permanent GPS station is the result of long-period phenomena of the site (tectonic motion, tides etc.; Teferle *et al.* 2008; Davis *et al.* 2012; Chen *et al.* 2013) and the long-period noise of the GPS time-series (<0.1 Hz; ionosphere, multipath, etc.; Mertikas & Damianidis 2007; Psimoulis & Stiros 2012), while the standard error expresses the precision of the GPS time-series.

The instantaneous displacement d_i of the epoch i is computed with respect to the mean average u_{mi}:

$$d_i = u_i - u_{mi}. \tag{3}$$

The noise level of the GPS time-series n_i is a function of the standard error and of parameter k, which defines the amplitude of the threshold, given by the expression (Fig. 2c)

$$n_i = k \cdot \sigma_i. \tag{4}$$

We compare the noise of the time-series n_i against the displacement d_i (Fig. 2c). If the norm of the instantaneous displacement $|d_i|$ is larger than the noise level n_i, it means that the short-period displacement d_i is larger than the corresponding long-period noise level and d_i can be flagged as 'potential displacement', otherwise the algorithm initialize for the next epoch $i + 1$.

However, in case of 'potential displacement' at epoch i, which might be the result of site-specific anomaly, due to GPS error (i.e. cycle slip, multipath, interference, etc.) or local ground instability (i.e. unstable foundation, etc.), the algorithm searches for consistent detection of 'potential displacement' at other GPS stations, which are lying in a distance less than R from the station q of the detected 'potential displacement' within the next T seconds (Fig. 2d). The time interval of T seconds is given by the following equation:

$$T = \frac{R}{V}, \tag{6}$$

where V corresponds to the velocity of the seismic surface waves (i.e. Rayleigh, Love). Practically, the time interval T expresses the needed traveltime of the seismic surface waves to spread to the entire examined neighbouring GPS station area. Since the surface waves are assumed as the relative slowest seismic waves (Shearer 1999), this time period corresponds to the maximum period in which the seismic signal should be detected at neighbouring stations.

To avoid potential inconsistencies in the detection due to GPS site-specific dependencies and local effects (e.g. GPS signal outliers, local sky-view masks, bedrock instability), the algorithm computes the ratio of the number of the GPS sites, in which consistent 'potential displacement' is detected, to the total number of the neighbouring GPS stations. If this ratio is higher than a pre-defined threshold w, which ranges between 0 and 1, then the 'potential displacement' corresponds to real seismic displacement, otherwise the algorithm initialize from the beginning for the next epoch $i + 1$. However, if there is continuous result of 'potential displacement' from a specific GPS site or a group of GPS sites, but still the ratio is lower than the threshold, this would be the result of real displacement due to local ground displacement or foundation instability or result of artefact of the GPS solution due to weak satellite constellation (Mao *et al.* 1999; Williams *et al.* 2004; Msaewe *et al.* 2017), signal interference (Williams *et al.* 2004; Wu *et al.* 2015) or cycle slip and re-convergence of the PPP solution (in case of one GPS-site only; Li *et al.* 2011). In the above cases, the local or site-specific anomaly observed in the GPS solution will be flagged but not as seismic motion.

Furthermore, during the spatial search there is no correlation between the directions of the detected displacement of the GPS sites. Hence, there is no evaluation whether the detected displacement follow a specific patter, which would reflect the ground deformation due to a specific fault type (normal, strike-slip, etc.). Potentially, for specific GPS networks in an area of well-known and studied seismic faults, this correlation could be applied, limiting even further the false alarms.

In this study, the performance of RT-SHAKE is evaluated in detecting the arrival of the seismic waves using only the GPS network records of the $M_w 9.0$ Tohoku-Oki 2011 earthquake, producing ground motion of various amplitudes (from few cm up to m)

along the GPS network. The performance of RT-SHAKE is assessed against the corresponding estimated time arrival from the strong motion networks of Japan, KiK-net and K- NET.

3 DATA

3.1 Strong-motion data

The strong-motion networks K-NET (Kyoshin network) and KiK-net (KIBAN kyoshin network), both operated by the National Research Institute for Earth Science and Disaster Prevention, consist of 1034 and 669 seismometers, respectively (Aoi *et al.* 2011). The K-NET stations are installed on thick sediments, while the KiK-net stations are located on rock or thin sediments, as they are designed for highly sensitive seismic observation (Aoi *et al.* 2004). Furthermore, the K-NET stations are installed at the ground surface, while the KiK-net stations are consisted of two sensors, one installed on ground surface and the other at the bottom of the boreholes of 100–200 m depth.

Both networks consist of the same instrumentation, using V403 or V404 tri-axial force-balance accelerometer (450 Hz frequency and 0.707 damping factor). The recording frequency of the sensors is 100 Hz, with pre-set triggering thresholds of 2 and 0.2 s^{-1}gals for the K-NET and KiK-net sensors, respectively (Aoi *et al.* 2004). The minimum and maximum durations are 120 and 300 s, respectively, including 15 s of pre-triggering data.

The earthquake of $M_w 9.0$ Tohoku 2011 was successfully recorded by both networks, with available strong-motion records from 700 KiK-net sites and 525 K-NET sites. The records, consisted of north, east and vertical component for each site, were of 100 Hz recording frequency and duration up to 300 s. The acceleration of the each site derived by correcting the raw data from the gain and transforming the recording time, which was initially given in UTC time (i.e. time difference of 15 leap seconds) into GPS time. Only the ground surface sensors of the KiK-net were used for the analysis, in order to be consistent with the records of the K-NET and GPS.

3.2 GPS data

The GNSS network of Japan, which is known as GNSS Earth Observation Network System (GEONET-Japan) and operated by the Geospatial Information Authority of Japan, consists of more than 1200 continuously observing GNSS stations, covering the Japanese land area with 20 km average distance between neighbouring GNSS sites (Sagiya 2004).

The $M_w 9.0$ earthquake of Tohoku on 2011 March 11 was fully recorded by GEONET. GPS records from 847 GEONET stations of 15-hr duration and 1 Hz sampling rate, covering the period of the earthquake, were available. The GPS records have been processed using the scientific Bernese GPS Software 5.2 (Dach *et al.* 2007). The data were post-processed in a Precise Point Positioning (PPP) mode using *a priori* information of highest quality from the Center for Orbit Determination in Europe (Bock *et al.* 2009; Dach *et al.* 2009) resulting to the displacement time-series in north, east and up components of 1 Hz sampling rate. The minimum elevation angle of the processing was 15° to avoid the impact of the low satellites (i.e. multipath, troposphere, etc.) which could limit the GPS data quality (Kawamoto *et al.* 2016)

4   RESULTS

4.1   Noise level and ground response based on the GPS data

A preliminary analysis of the GPS time-series was conducted to estimate the noise level of the GPS records, which were then used to define the thresholds for the detection algorithm. More specifically, the GPS time-series of the Tohoku-Oki M_w9.0 2011 earthquake were analysed to estimate the noise level of each GPS component (north, east and vertical), computed as the standard deviation of 10-min period prior to the time of the earthquake. In Fig. 3(a) are presented the histograms of the noise level of each component of the GPS sites, where for their majority the noise level of east and north components does not exceed the 3–4 mm, while for the vertical component does not exceed 7–8 mm. The analysis of the RTK solutions of the same GPS records, which are in real-time and used in Wright *et al.* (2012), resulted to similar noise level for all the components (Fig. 3b), indicating that both GPS solutions (real-time and simulated PPP near real-time) achieved similar accuracy expressed by the same noise level.

Furthermore, the analysis of the GPS PPP and RTK solutions for 10 and 50 s after the time of the earthquake (t0) indicates that (i) for t0 + 10 s there is no evidence of ground response in the GPS data, as the seismic waves had not reached the locations of the GPS sites at that moment, reflecting that the GPS data are in the corresponding noise level and (ii) for t0 + 50 s there is strong ground response above the noise level for ~70 GPS sites of the GPS network, which cover the area up to 250 km from the epicentre, which are expected to be affected for the given time-period from the propagation of the seismic waves. Thus, it seems that the GPS time-series can express reliably the ground response, exceeding the noise level in case of strong ground motion, and reflect the impact of the propagation of the seismic motion through the GPS network. Also, the agreement between the amplitude of the ground response for the two different GPS solutions (i.e. simulated Bernese-PPP near real-time and RTK solution) reveals the reliability of the GPS estimation for the strong ground motion, regardless the processing mode (i.e. PPP near real-time, real-time).

4.2   Detection by strong-motion networks

From the application of the STA/LTA algorithm to the strong-motion records derived the triggering time and the corresponding acceleration time-series. Based on the analysis and the plots of the triggering time of the strong-motion sensors versus their corresponding distance from the epicentre, where as positive and negative distance is expressed the distance of the sites northern and southern from the epicentre respectively, we find that (Fig. 4):

(1) linear trend of the detection of the seismic wave is observed both for the K-NET and KiK-net networks, but is more uncertain with the increase of the distance from the epicentre.

(2) The linear trends of the two networks slightly deviate, indicating the difference in the detection of the seismic wave propagation. Specifically, the detection of the KiK-net network seems to be slightly faster and more sensitive due to the different triggering mechanism of the KiK-net sensors (Figs 4a and b).

(3) There are sites where the strong-motion sensors show delayed triggering (Figs 4a and b; symbolized by triangles). The delayed triggering could be due to malfunction of the corresponding sensors, attenuated seismic signal or even local effect. The majority of the delayed-triggered strong-motion sensors corresponded to records of duration less than 250 s.

For the current study were used only the strong-motion sensors with duration of 300 s and consistent triggering following the linear trend, in order to make objective comparison with the GPS network detection.

## 4.3   Detection of spatially consistent motion by a GPS network

The RT-SHAKE algorithm was developed in the framework of Bernese GPS Software 5.2 and was applied separately to each component (north, east and up) of the 847 available GPS sites time-series. The method was specified for the detection of the seismic motion of Tohoku M_w9.0 earthquake using the Japan GEONET data. Five parameters of the algorithm were defined based on previous studies and the characteristics of the GPS network of the case study. More specifically, the parameters which were defined are:

(1) the number of epochs $m = 80$. The parameter m was used to limit low-frequency noise (i.e. <0.1 Hz) of the GPS time-series and was based on models of GPS noise (Teferle *et al.* 2008; Psimoulis & Stiros 2012; Moschas & Stiros 2013) and the corresponding parameter of similar studies (Allen & Ziv 2011; Colombelli *et al.* 2013).

(2) The threshold $k = 3$, which defines the threshold for the motion detection. The defined values k corresponds to the $\pm 3\sigma$-zone which expresses a conservative noise zone of the GPS time-series defined by the 99 per cent data of for the given interval (Psimoulis & Stiros 2012); value exceeding this zone is not considered as regular time-series noise, but as outlier or potential displacement signal. The noise zone of the GPS time-series did not exceed the limit of 1.5 cm, suggested as threshold of the early-warning system by Colombelli *et al.* (2013).

(3) The radius of the searching area $R = 30$ km. The radius selection is consistent with the 20 km station-distance design of the GPS network in Japan (Sagiya 2004) and limits the cases where the searching area consists of less than three stations, in order to avoid false alarms (Kawamoto *et al.* 2017) and retain also the fast performance of the detection.

(4) The seismic velocity $V = 3$ km s^{-1}. This parameter is based on the typical low limit of the velocities of the surface waves (Shearer 1999), as observed for the 2011 Tohoku-Oki event.

(5) The threshold $w = 0.8$ for the first GPS station detection, which is relatively high in order to make the algorithm robust, and $w = 0.6$ for the rest GPS stations, to enhance the sensitivity the detection for the GPS sites far from the epicentre where the seismic signal is attenuated and local-site effects may influence the GPS records. The threshold w was defined based on the geometry and density of the GPS network and after several tests.

From the kinematic time-series of the 847 GPS stations derived the detection of the seismic signal, expressed in time with reference the official USGS earthquake time. The first detection of seismic signal is completed using the data collected by the GPS station 0550 (Supporting Information Fig. SA2), the closest GPS site to the epicentre, 23 s after the official USGS earthquake origin time (05:46:24 UTC, http://earthquake.usgs.gov/earthquakes/eqin thenews/2011/usc0001xgp/) and about 7 s after the detection of the collocated strong-motion K-NET site MYG011 (Lat: 38.30119, Long: 141.50069). The seismic displacement was first detected at the east component of the GPS time-series with amplitude 1.1 cm
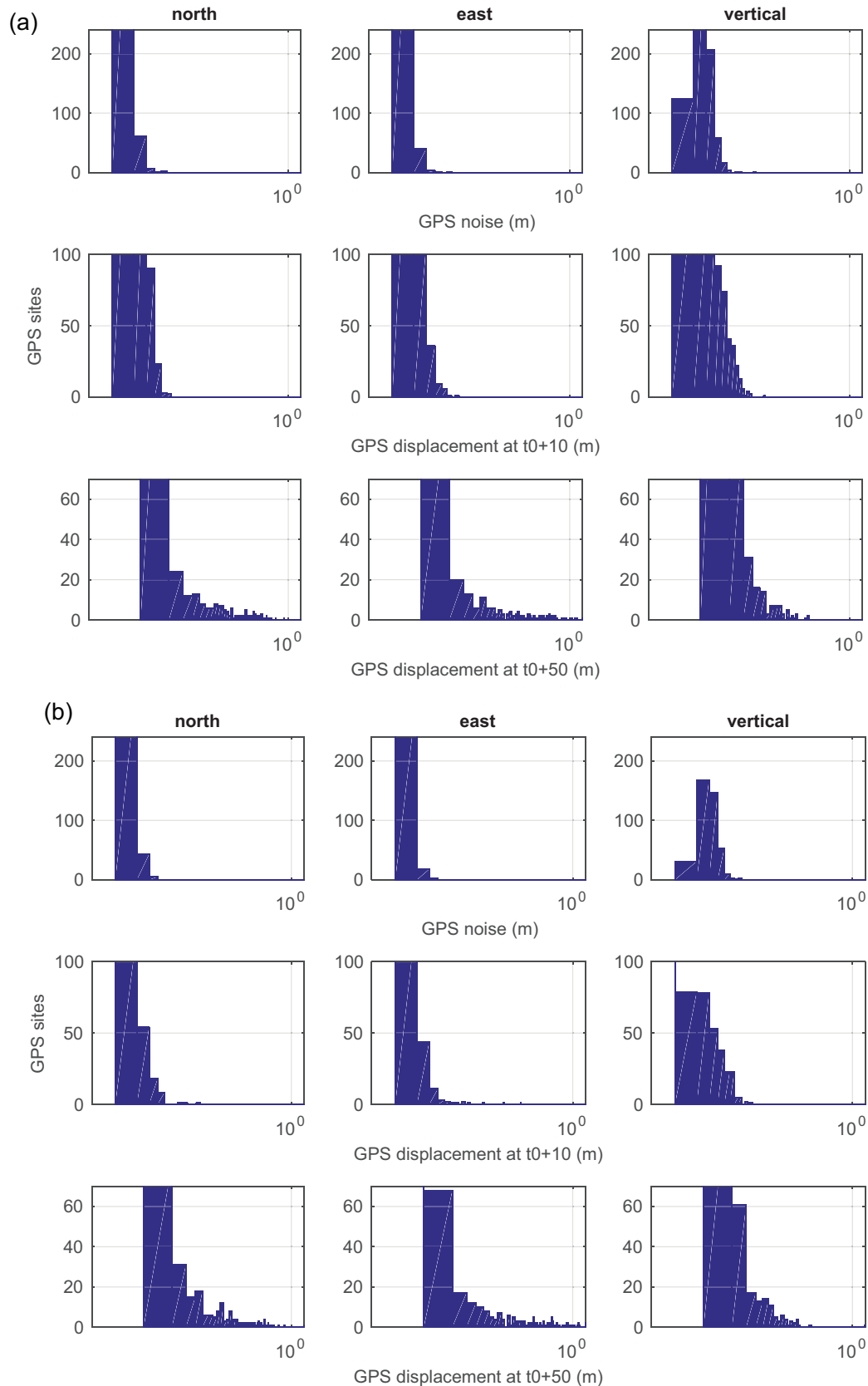
Figure 3. (a) Noise level of GPS time-series (upper row), compared to the measured amplitude of the ground motion at 10 s (middle row) and at 50 s (lower row) after the origin t0 of the earthquake, based on the Bernese–PPP solution. (b) As panel (a) for GPS time-series derived from solutions of Wright *et al.* (2012).
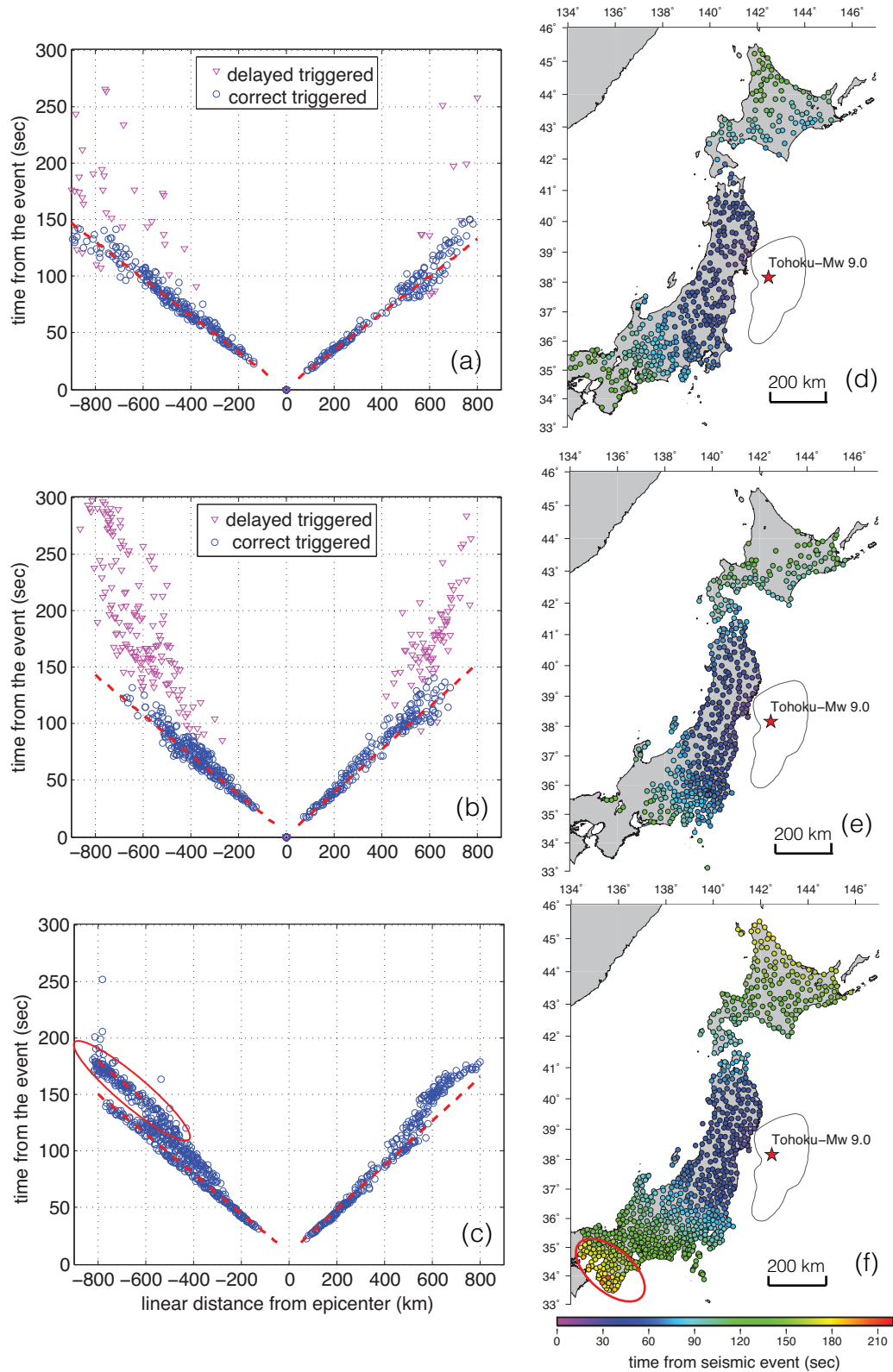
Figure 4. The detection time of the seismic signal for the (a) KiK-net and (b) K-NET strong motion networks referenced to the origin earthquake time versus the corresponding linear stations distance from the epicentre. Negative and positive distances are considered the distances of the southern and northern stations from the epicentre, respectively. The propagation of the earthquake is consistently detected by the seismic network. The circular and triangular stations correspond to correct and delayed triggered stations, respectively. The red dotted lines express the linear trends of the detections. (c) The detection time of the seismic signal by the GPS network, referenced to the origin earthquake time versus the corresponding linear station distance from the epicentre. The red dotted lines indicate the three clusters of linear trends. The third cluster (in the ellipse) is parallel to the primary linear trend with a time delay of 35 s. The maps of propagation of the seismic signal as it is detected by the (d) KiK-net, (e) K-NET and (f) GPS networks. The ellipse includes the GPS sites of cluster of the third linear trend.

(d_i), while the corresponding noise level (n_i) was of ~0.9 cm (σ_i ~0.3 cm).

The performance of the detection algorithm for various values of the parameters m (10–150), k (2.5-4), R (20–40) and w (0.4–1) was also examined. The detection results were not significantly affected by the variation of the parameters k and R, apart from some GPS sites mainly far from the epicentre and/or isolated GPS sites. The reduction of the parameter w to values below 0.5 led to partly unreliable seismic signal detection especially for the regions of the network far from the epicentre ($R > 400$–500 km), where the seismic signal is attenuated. Regarding the parameter m, it was observed that for values lower than 30 (i.e. 30 s window) or higher than 120 (i.e. 2 min window), the low-frequency noise of the GPS time-series was not modelled effectively, leading to overestimation of the low-frequency noise and delays in motion detections (for low m) or underestimation of the low-frequency noise, which was not filtered properly causing false detection, respectively.

Generally, from the five parameters of the RT-SHAKE algorithm, parameters w and R are network-specific, parameter m depends on the GPS noise characteristics, which can be GPS site-specific and parameters k and V follow commonly applied techniques and assumptions. Thus, mainly the parameters (w, m, R) should be adjusted based on GPS time-series and the GPS network of the monitoring application, in order to limit the impact of the GPS noise and have adequate number of GPS sites (three based on this case study) on the spatial search to avoid the false detections.

5 ANALYSIS AND COMPARISON OF GPS WITH STRONG-MOTION DATA

The comparison of the detection times of ground motion by the two strong-motion networks (KiK-net and K-NET) and the GPS network shows similar pattern of propagation of the seismic signal through the networks (Figs 4a–c) with clear differences though between the detection times of the three networks, reflected also in the corresponding linear trends. Specifically, the linear trends of the southern and northern KiK-net network of the epicentre correspond to velocities of 6.15 and 6.08 km s^{-1}, respectively, while the corresponding velocities for the K-NET network are 5.93 and 5.85 km s^{-1}, respectively. For the GPS network, the corresponding apparent velocities of the linear trends are 5.81 m s^{-1} and 5.70 km s^{-1}, respectively. The difference of the velocities between KiK-net and K-NET networks is due to the lower triggering mechanism and higher sensitivity of KiK-net sensors. As expected, the GPS detection proves to be less sensitive but still consistent with the detection of the strong-motion networks.

The main difference between the GPS and the strong-motion network-based detections resides in the presence of a second linear trend which appears in the southern GPS sites for >600 km distance from the epicentre (Fig. 4c). This linear trend cluster is parallel to the linear trend cluster of the rest of the southern GPS sites, corresponding to velocity 5.8 km s^{-1}, appearing though a time delay of ~35 s. The same estimated velocity of the two clusters means that these GPS sites detect seismic wave of the same type. The relative large time difference of 35 s excludes the possibility of detecting reflective or refracted seismic waves by the second cluster sites (Shearer 1999), reinforcing the possibility of detecting a second seismic event, which triggered the south-eastern GPS sites of the network (Fig. 4f; GPS sites in the ellipse).

The latter is consistent with the suggestion that the Tohoku 2011 earthquake consisted of more than one rupture events (Koketsu

et al. 2011; Suzuki et al. 2011; Maercklin et al. 2012). The common conclusion of the studies of Suzuki et al. (2011) and Koketsu et al. (2011) is the existence of three ruptures, with the first two of them close to the epicentre of the main shock and the third one south-southwest from the initial epicentre in a distance of ~150–180 km (Koketsu et al. 2011). More specifically, Suzuki et al. (2011) proposed that the Tohoku-Oki rupture was composed of three slip patches, as they observed two distinct wave groups with 40 s relative time difference and a third distinct wave group propagating from Fukushima prefecture, about 50 s after the first rupture, in a longitudinal section parallel to the fault rupture (see fig. 2 in Suzuki et al. 2011).

Following the same approach with Suzuki et al. (2011) and making the corresponding section at the GPS network, the displacement waveforms of the EW component were formed, ordered by station latitude (Fig. 5a). Based on the detection time and the GPS displacement waveform is observed:

(1) a parabolic pattern of detection, reflecting the parabolic propagation of the seismic signal along latitude similarly with that derived from Suzuki et al. (2011) and

(2) a two-step response pattern at the stations of the Miyagi prefecture (Fig. 5b), expressing the response of the sites caused by the two successive ruptures.

The time difference of the two-step responses is approximately ~40 s, as they are defined by the two parabolic curves (Fig. 5b), which is more evident for the GPS sites close to the Miyagi prefecture (GPS site 0550; Supporting Information Fig. SA2), which again confirms that the second step response is not seismic wave reflection. Additionally the relative displacement of the two responses reveal that the second rupture was dominant to the east direction and decreases drastically as moving away from Miyagi prefecture, satisfying the propagation of the model of the second rupture by Koketsu et al. (2011).

For more direct and objective comparison of the detection of the three networks, the reduced traveltime of the seismic signal was computed. More specifically, the reduced traveltime for each site of every network is given by the following expression:

$$t_{\text{red}} = t - \frac{d}{v_{\text{ref}}}, \tag{7}$$

where t is the detection time with reference the origin earthquake time, d the distance of the site from the epicentre and v_{ref} the reference velocity of the seismic signal propagation. Practically, the reduced traveltime expresses the relative delay of the detection having as reference the required traveltime of a seismic wave. In our analysis the reference velocity was 6.15 km s^{-1} corresponding to the highest velocity of the linear trends, detected by the KiK-net network. By plotting the reduced traveltime versus epicentre distances for the three networks (Fig. 6a) and the corresponding time detection of the networks map (Fig. 6b), it is clear that:

(1) the time delays between the GPS and the strong-motion networks KiK-net and K-NET are ~10 and ~5 s, respectively. The time delay remains constant for distance up to 300 km from the epicentre.

(2) The GPS detection delay increase with the distance from the epicentre (>400 km) due to the attenuated displacement seismic signal for sites far from the epicentre.

(3) The seismic signal detections become more scatter with the increase of the distance. The latter is more evident for the northern sites and distances >400 km from the epicentre.
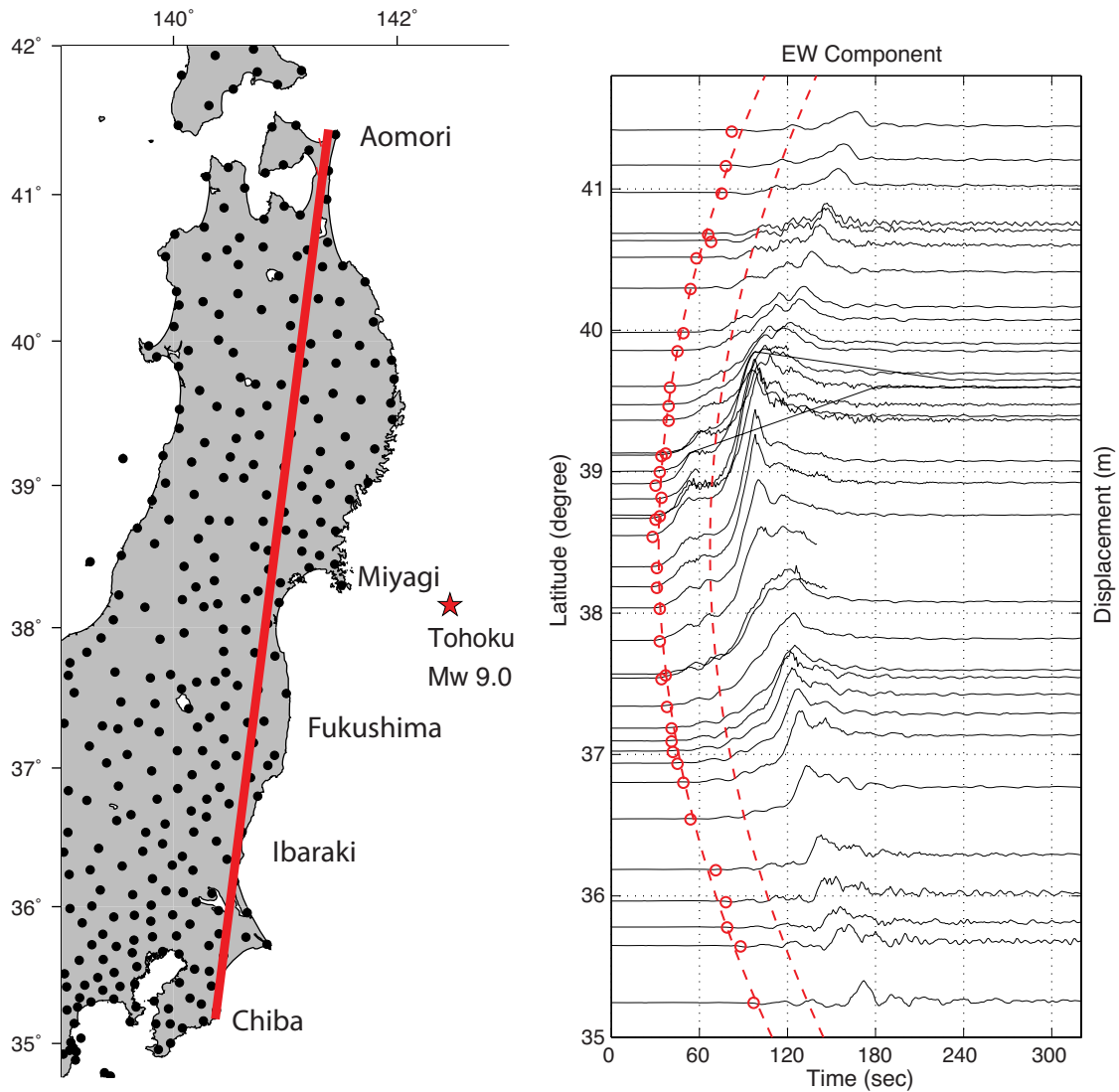
Figure 5. Left panel: the GPS network map with the red line indicating the examined section similar to that of Suzuki *et al.* (2011). Right panel: the plot of the EW component of the displacement time-series of the section GPS sites ordered by latitude. The circles indicate the detection time for each site and the fitted parabolic dotted line approaches the parabolic propagation of the seismic signal along the section. The second dotted line is shifted by 40 s from the first for the indication of the second rupture according to Suzuki *et al.* (2011).

(4) There are strong-motion sites corresponding to higher velocity than the reference, especially northwards from the epicentre (black dots in Fig. 6b).

6 FALSE ALARMS

To evaluate the robustness of the RT-SHAKE algorithm and its effectiveness in avoiding false alarms, the algorithm was applied in the ~4-hr period before the earthquake, corresponding to 15 000 GPS samples (i.e. 1 sps). For the given period, potential flagged alarm could be considered as false alarm, since there was no documented ground motion. Using the same parameters as for the detection of the seismic motion propagation, there were nine events of false alarms in the ~4-hr period. The nine false alarms occurred totally in 17 GPS sites (Table 1; Fig. 7), with six false alarms occurring in four GPS sites (GPS sites 0582, 0583, 0627, 2110). Furthermore, in all cases of false alarms there were at least two GPS stations, which fulfilled the two conditions of the algorithm ($d_i > n_i$ and $w > 0.8$

or 0.6), with apparent displacement ranging between 1 and 2 cm. The GPS stations of the false alarms were at the south-eastern part of the GPS network (i.e. close to Tokyo), where the density of the GPS network is significantly high.

The false alarms seemed to be the result of local effects, which had impact in relatively closely spaced GPS sites and led to poor quality of GPS solution, producing anomalies in the time-series, which cannot be modelled and are identified as potential ground motion (Msaewe *et al.* 2017). More specifically, in most false alarm events, which were triggered systematically by specific GPS sites (i.e. 0582, 0583, 0627, 2110), the azimuth of the detection motion was continuously decreasing with time, indicating that the shift of the detected motion can be related to the satellite constellation (Houlié *et al.* 2011). Hence, the apparent detected motion could be the result of the impact of a satellite signal and/or potential local interference in the GPS solution, as the azimuth of the detected motion-anomaly on the GPS solution follows the movement of the problematic satellite on its orbit. For instance, for the GPS
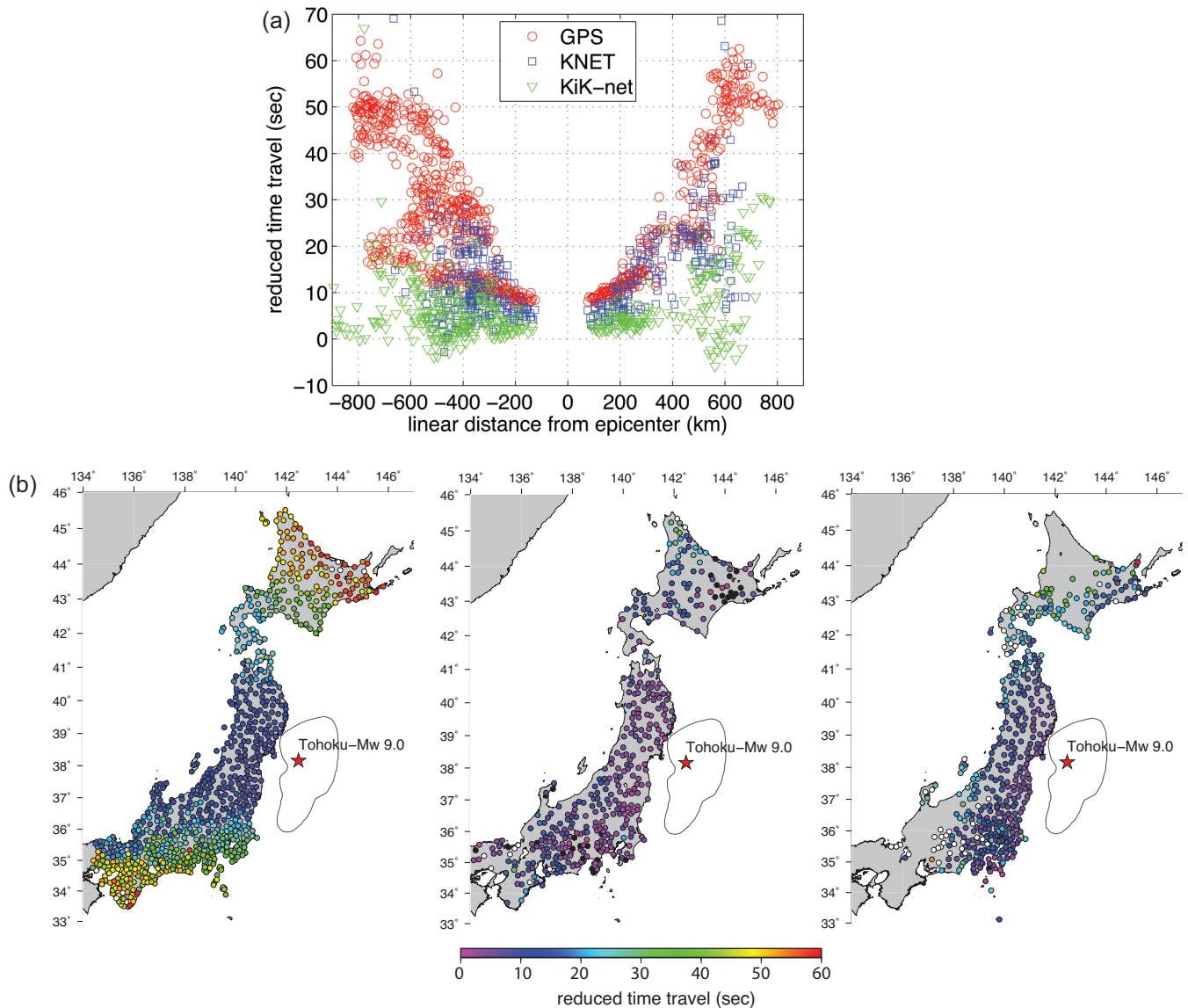
Figure 6. (a) The plot of the reduced traveltime versus the distance from the epicentre for the network of KiK-net (triangles), K-NET (squares) and GPS (circles). (b) The (1) GPS, (2) KiK-net and (3) K-NET network maps with the reduced traveltime estimations. The white dots correspond to reduced traveltime larger than 60 s, while the black dots correspond to reduced traveltime less than 0 s.

sites 0583, 0582, 0627 and 2110 which are closely spaced (in-between-distance less than 30 km), the azimuth of the falsely detected ground motion decreases constantly about 10°–13° (azimuth ranges between 108° and 123° for the four GPS sites), indicating that both GPS sites are apparently affected by the same problem of the satellite constellation.

To enhance the performance of the RT-SHAKE algorithm and make it more robust, an additional (third) check could be to correlate the detected motion with the time-series of the dilution-of-precision (DOP) values of the satellite constellation and the signal-to-noise (SNR) of the satellite signals. More specifically, the DOP values and the SNR, which express the quality of the satellite constellation and the satellite signal, respectively, indicate potential sudden changes which could affect the GPS solution. In case the detected motion coincides with the sudden change of DOP and/or SNR values, then this would indicate that the detected motion is the artefact of poor GPS solution.

7 DISCUSSION

It is shown that the RT-Shake time delays are the result of: (i) the time required (15 s) for the seismic waves to reach the GPS antenna's location and (ii) the required time for the accumulation of the displacement above the noise level of the GPS data, which depends on the distance from the epicentre and the strength of the seismic event, as the displacement is associated mainly with S and surface waves. However, both limitations could be addressed by densification of the GPS networks. The high GPS noise level relatively to the low strong-motion sensor noise level results to the time delay of the seismic signal detection by the GPS relatively to that of the strong-motion detection. Indicative is the case of the GPS site 0550 (Supporting Information Fig. SA2), which is issuing a motion warning ∼7 s after the detection of collocated strong-motion sensor (MYG011), due to the accumulated displacement above the noise level (∼1 cm). However, the current time delay of the GPS detection is consistent and even slightly smaller than

Table 1. The list of the GPS sites, which triggered false alarms, where it is presented their location (latitude, longitude), the number of the false events for each GPS site and the range of the amplitude and the azimuth of the falsely detected ground motion by each GPS site.

GPS site	Latitude	Longitude	False events	Range of detected motion (mm)	Range of azimuth (degrees)
0582	36.30071	139.98777	6	12.3–15.1	119°–109° (decreasing)
0583	36.11481	139.93150	6	13.4–15.8	121°–108° (decreasing)
0627	36.10364	140.08631	6	12.9–14.2	123°–110° (decreasing)
2110	36.10612	140.08719	6	12.2–13.9	125°–113° (decreasing)
0230	35.26860	139.14242	5	12.5–14.5	164°–148° (random)
3068	35.24552	139.04934	5	11.8–14.9	76°–63° (decreasing)
3038	35.32160	138.88165	4	12.0–13.8	153°–148° (random)
3025	35.54414	140.18656	3	10.5–12.3	163°–144° (decreasing)
3069	35.44358	138.60687	2	13.9–15.4	123°–130°
3073	35.28946	138.44570	2	13.5–14.3	133°–132°
3002	36.26327	140.17426	2	13.6–14.2	138°–147°
0981	35.46769	138.60687	2	11.7–12.3	177°
3037	35.33314	140.14679	1	12.3	106°
0606	35.64952	138.69038	1	15.9	105°
3075	35.20318	138.61699	1	11.8	108°
3076	35.17359	138.72154	1	15.7	107°
0248	35.74688	138.69513	1	12.4	21°
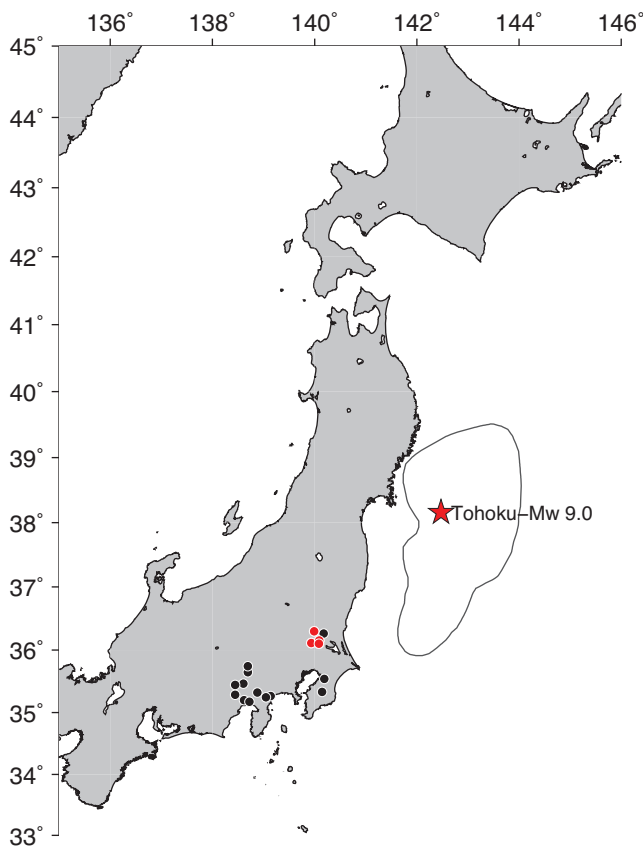
Figure 7. Map of the GPS sites where the false alarms occurred. Red are highlighted the GPS sites with the most (i.e. four) false alarms (0582, 0582, 0637 and 2110).

that of other studies (Colombelli *et al.* 2013), mainly due to the second spatial check, which allows to lower of the noise level of the GPS time-series by retaining simultaneously the robustness of the algorithm.

Largest time delays are observed in the northern GPS network (Fig. 6b), which reaches up to 50 s far from the epicentre (800 km; Fig. 6a) and can be explained by the strong directivity of the source

pulse propagation in the east direction (Koketsu *et al.* 2011). The directivity made less effective the detection by the GPS network relative to the more sensitive KiK-net and K-NET. Furthermore, the propagation of the rupture towards the east and the location of the third rupture southwards from the first two (Koketsu *et al.* 2011; Suzuki *et al.* 2011) explain the slightly smaller propagation velocities of the northern network than the southern. The few KiK-net sites, illustrated as black dots in Fig. 6(b), correspond to detection of seismic wave of higher velocity than the reference; the latter is probably the result of the faster propagation of the first rupture northwards (Koketsu *et al.* 2011), which is detected.

The time delay between the GPS and the strong-motion network detection times confirms the higher noise level of PPP GPS (∼1 cm) than the seismic sensors for real-time detection. Potentially, a smaller magnitude (i.e. $M_w 7.0$) occurred at the location of the Tohoku 2011 earthquake could have been detected with greater delay, as more time would be required for the accumulation of ground motion to exceed the threshold of the GPS noise level; this was the case for the study of Allen & Ziv (2011) for the El-Mayor Cucapah $M_w 7.2$ 2010 earthquake case study.

Regarding the seismic wave propagation velocities, the highest one derived by the KiK-net network (6.15 km s^{-1}), corresponding to typical velocity of *P*-wave of earthquake (Shearer 1999), and indicates that the KiK-net network detected the *P*-wave of the seismic signal. The group velocities of the GPS network linear trend (Fig. 6a) is slightly lower (5.8 km s^{-1}), suggesting though that the GPS network detects the accumulated displacement which corresponds to the *P*-wave signal.

By plotting the GPS detection at the time history of the radial displacement of the GPS sites versus epicentre distance (Supporting Information Fig. SA3) derives the consistent detection of the seismic wave for <400 km distance from epicentre, while for larger distances the detection pattern keeps following the seismic wave propagation and becomes more complicated mainly due to the several ruptures and the mixture of several seismic signals. More specifically, in northern GPS network, where there is strong attenuation of the seismic signal due to the directivity of the rupture, the GPS network detects, for distance larger than 400 km from the epicentre, seismic signal of lower velocity than *P*-waves, as soon as the displacement exceeds the noise level. On the contrary, the southern
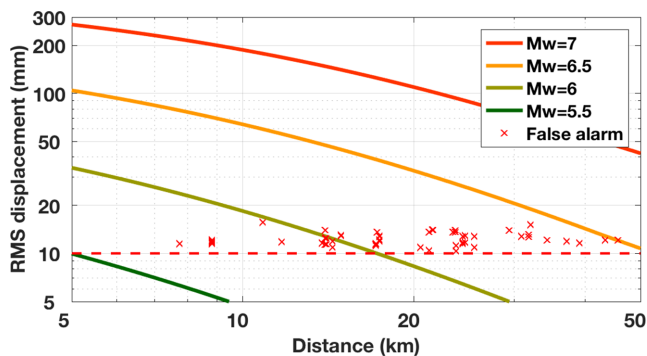
Figure 8. The static displacement of various magnitudes versus the distance from the epicentre, based on the ground motion prediction model (stochastic model) for Japan (Poggi *et al.* 2013), as used in Michel *et al.* (2017). The false alarms correspond to the distances between the GPS sites, which triggered the false alarms, and the detected displacement, which falsely triggered the algorithm.

GPS network detected reliably the seismic signal, which corresponds to the *P*-waves of the first rupture even for GPS sites (southwestern end of the GPS network) >600 km far from the epicentre, where the static displacement signal was rather low (<5–10 cm) and close to the noise level. The developed detection algorithm, using the noise level and spatial checks, allowed the consistent and coherent detection of the seismic displacement through the GPS network, indicating also through the detection the spatial characteristics of the seismic wave propagation.

Finally, by using the ground motion prediction model (GMPE; stochastic model) for Japan (Poggi *et al.* 2013) it can be determined the root-mean-square (RMS) displacement, using the static motion above 20 s where the displacement spectrum is flat, and how the RMS displacement varies with the distance from the epicentre (Fig. 8). Based on the GMPE, the average noise level (~1 cm) of the GPS sites and the density (~20 km) of the current GPS network, the GPS network could detect seismic motion for earthquakes >M_w6.0. By considering though the false detections of the GPS network (Table 1) and based on the assumption that the potential earthquake indicated by the false alarms are located in the middle of the triggered GPS sites, the lowest threshold of the earthquake magnitude where the RT-SHAKE algorithm can be used reliably is for magnitude >M_w6.5. However, the performance of the RT-SHAKE algorithm and the lowest threshold of the earthquake magnitude, where the algorithm can be used, depend on the GPS network geometry and the quality of the GPS solutions.

8 CONCLUSION

We successfully present RT-SHAKE, an algorithm designed to detect surface motions using GNSS real-time data streams. The testing and calibration of RT-SHAKE using Tohoku M_w9.0 2011 earthquake data set revealed that the GPS network data can be used to detect ground motion larger than 1–2 cm with great robustness; the displacements of the ground motion may correspond to a wide range of geohazards (e.g. large earthquakes, landslides, cliff collapses, etc.). RT-SHAKE based on GPS data proved to be consistent with results derived by the KiK-net and K-NET strong motion networks and due to the exceptional dimensions of the Tohoku-Oki 2011 earthquake, the GPS network detected displacements corresponding to *P*-waves. The delay of ~5–10 s in the detection of the

ground motion relatively to the strong motion networks due to the higher noise level of the GPS time-series.

The two-stage checks of the RT-SHAKE algorithm aim to eliminate the false alarms by resolving problems of outliers or GPS site-specific effect. The checks of the RT-SHAKE algorithm manage to limit the false alarms to nine for the period prior to the earthquake, corresponding to GPS time-series of ~15 000 samples. The false alarms still occur, due to triggering by GPS-sites, which are affected by poor satellite constellation or problematic satellite(s) (Msaewe *et al.* 2017). However, this weakness can be resolved by using additional parameters, such as the DOP values or the SNR of the satellite signals, to evaluate whether a potential detected motion is real or an artefact of the GPS solution due to the satellite constellation, the satellite signal and/or local interference (Msaewe *et al.* 2017; Peppa *et al.* 2018). Additional techniques for the long-term analysis of the GPS time-series, such as neural networks, may be used to enhance the modelling of the GPS time-series and limit number of false alarms (Kaloop & Hu 2015). Since the algorithm is developed to be able for application also in other sensors (i.e. seismic sensors, tiltmeters, etc.), potential triggered GPS sites could be spatially checked with additional sensors of other monitoring networks, to limit even further the false alarms.

The developed algorithm can be used not only for the detection of the ground deformation due to earthquakes, but also for the direct monitoring of other types of geohazards related to motion (e.g. landslides, tsunamis, volcanoes), through the detection of the propagated motion. The GPS detection may be delayed with respect other sensors (i.e. seismic sensors, accelerometers, etc.), but still provide prompt information about the severity and the spatial characteristics of a given event. Following appropriate modifications the same code may be applied to real-time data from seismic data and/or other sensors to monitor geohazards.

The developed method and its parameters were adjusted for the GEONET-Japan network dense network and this megaearthquake. Further improvements and adjustments may be required for its application in case of different GPS networks and earthquakes of smaller magnitude or for monitoring other types of ground deformation (i.e. landslides, geothermal activities, etc.).

In the future, the GPS ground motion detection could be further enhanced by using higher sampling rate (i.e. 5 Hz), which will refine the precision of the GPS detection, thanks to the enhanced time resolution, and allow more accurate estimations of ground motion and of the earthquake characteristics (Michel *et al.* 2017). For earthquakes close to the lowest threshold of $6.5 < M_w < 7$, the detection will be still achieved with similar coherency and consistency, with potential detection delay for the relatively small seismic ground motion. Thus, even though the relatively delay, the GPS network can perform coherently with the seismic network in early warning systems, and can supplement the existing seismic networks and contribute towards efficient EEW systems.

http://datahouse1.gsi.go.jp/terras/terras_english.html (last accessed June 2016). The KiK-net and K-NET data are provided by the National Research Insitute for Earth Science and Disaster Resilience (NIED).

REFERENCES

Allen, R.M., Gasparini, P., Kamigaichi, O. & Böse, M., 2009. The status of earthquake early warning around the world: an introductory overview, *Seismol. Res. Lett.,* **80**(5), 682–693.

Allen, R.M. & Kanamori, H., 2003. The potential for earthquake early warning in Southern California, *Science,* **300**, 786–789.

Allen, R.M. & Ziv, A., 2011. Application of real-time GPS to earthquake early warning, *Geoph. Res. Lett.,* **38**, L16310.

Allen, R.V., 1978. Automatic earthquake recognition and timing from single traces, *Bull. seism. Soc. Am.,* **68**(5), 1521–1532.

Aoi, S., Kunugi, T. & Fujiwara, H., 2004. Strong-motion seismograph network operated by NIED: K-NET and KiK-net, *J. Japan Assoc. Earthq. Eng.,* **4**(3), 65–74.

Aoi, S., Kunugi, T., Nakamura, H. & Fujiwara, H., 2011. Deployment of new strong motion seismographs of K-NET and KiK-net, in *Earthquake Data in Engineering Seismology. Geotechnical, Geological, and Earthquake Engineering,* Vol. **14**, pp. 167–186, eds Akkar, S., Gülkan, P. & van Eck, T., Springer.

Avallone, A. *et al.*, 2011. Very high rate (10 Hz) GPS seismology for moderate magnitude earthquakes: the case of Mw 6.3 L'Aquila (central Italy) event, *J. geophys. Res.,* **116**, B02305, doi: 10.1029/2010JB007834.

Benoit, L., Briole, P., Martin, O., Thom, C., Malet, J.P. & Ulrich, P., 2015. Monitoring landslide displacements with the Geocube wireless network of low-cost GPS, *Eng. Geol.,* **195**(1), 111–121

Bertazzi, P.A., Zoccheti, C., Pesatori, A.C., Guercilena, S., Sanarico, M. & Radice, L., 1989. Ten-year mortality study of the population involved in the Seveso incident in 1976, *Am. J. Epidemiol*., **129**, 1187–1200.

Blewitt, G., Hammond, W.C., Kreemer, C., Plag, H.-P., Stein, S. & Okal, E., 2009. GPS for real-time earthquake source determination and tsunami warning systems, *J. Geod.,* **83**(3–4), 335–343.

Blum, P.A., Jobert, G. & Jobert, N., 1959. Premiers résultats obtenus à l'aide d'inclinomètres, *C. R. Hebd. Seances Acad. Sci.,* **248**, 1551–1554.

Bock, H., Dach, R., Jäggi, A. & Beutler, G., 2009. High-rate GPS clock corrections from CODE: support of 1 Hz applications, *J. Geod.,* **83**(11), 1083–1094.

Bock, Y., Melgar, D. & Crowell, W., 2011. Real-time strong-motion broadband displacement from collocated GPS and accelerometers, *Bull. seism. Soc. Am.,* **101**(6), 2904–2925.

Bock, Y., Prawirodirdjo, L. & Melbourne, T., 2004. Detection of arbitrary large dynamic ground motions with a dense high-rate GPS network, *Geophys. Res. Lett.,* **31**, L06604, doi:10.1029/2003gl019150.

Bondarescu, R., Bondarescu, M., Hetenyi, G., Boschi, L., Jetzer, P. & Balakrishna, J., 2012. Geophysical applicability of atomic clocks: direct continental geoid mapping, *Geophys. J. Int.,* **191**, 78–82.

Bondarescu, R., Schärer, A., Lundgren, A., Hetényi, G., Houlié, N., Jetzer, P. & Bondarescu, M., 2015. Ground-based optical atomic clocks as a tool to monitor vertical surface motion, *Geophys. J. Int.,* **202**, 1770–1774.

Chen, Q., van Dam, T., Sneeuw, N., Collilieux, X., Weigelt, M. & Rebischung, P., 2013. Singular spectral analysis for modeling signals from GPS time series, *J. Geod.,* **72**, 25–35.

Cirella, A., Piatanesi, A., Cocco, M., Tinti, E., Scognamiglio, L., Michelini, A., Lomax, A. & Boschi, E., 2009. Rupture history of the 2009 L'Aquila (Italy) earthquake from non-linear joint inversion of strong motion and GPS data, *Gephys. Res. Lett.,* **36**, L19304, doi:10.1019/2009GL039795.

Colombelli, S., Allen, R. & Zollo, A., 2013. Application of real-time GPS to earthquake early-warning in subduction and strike-slip environments, *J. geophys. Res.,* **118**, 3448–3461.

Crowell, B.W., Bock, Y. & Squibb, M.B., 2009. Earthquake early-warning using total displacement waveforms from real-time GPS networks, *Seismol. Res. Lett.,* **80**(5), 772–782.

Dach, R., Hugentobler, U., Meindl, M. & Fridez, P. 2007. *The Bernese GPS Software Version 5.0,* Astronomical Institute, University of Bern.

Dach, R. *et al.*, 2009. GNSS processing at CODE: status report, *J. Geod.,* **83**(3–4), 353–366.

Davis, J.L., Wernicke, B.P. & Tamisiea, M.E., 2012. On seasonal signals in geodetic time series, *J. geophys. Res.,* **117**, B01403.

Doi, K., 2011. The operation and performance of earthquake early warnings by the Japan Meteorological Agency, *Soil Dyn. Earthq. Eng.,* **31**, 154–162.

Edwards, B., Allmann, B., Fäh, D. & Clinton, J., 2010. Automatic computation of moment magnitudes for small earthquakes and the scaling of local to moment magnitude, *Geophys. J. Int.,* **183**(1), 407–420.

Espinosa-Aranda, J.M., Cuéllar, A., Rodriguez, F.H., Frontana, B., Ibarrola, G., Islas, R. & Garcia, A., 2011. The seismic alert system of Mexico (SASMEX): progress and its current applications, *Soil Dyn. Earthq. Eng.,* **31**, 154–162.

Ferreira, S. & Karali, B., 2015. Do earthquakes shake stock markets? *PLOS One,* **10**, e0133319.

Fournier, N. & Jolly, A.D. 2014. Detecting complex eruption sequence and directionality from high-rate geodetic observations: the August 6, 2012 Te Maari eruption, Togariro, New Zealand, *J. Volc. Geotherm. Res.,* **286**, 387–396

Ge, M., Gendt, G., Rothacher, M., Shi, C. & Liu, J., 2008. Resolution of GPS carrier-phase ambiguities in Precise Point Positioning (PPP) with daily observations, *J. Geod.,* **82**(7), 389–399.

Geng, J., Bock, Y., Melgar, D., Crowell, B.W. & Haase, J.S., 2013a. A new seismogeodetic approach applied to GPS and accelerometer observations of the 2012 Brawley seismic swarm: implications for earthquake early warning, *Geochem. Geophys. Geosyst.,* **14**(7), 2124–2142.

Geng, J., Melgar, D., Bock, Y., Pantoli, E. & Restrepo, J., 2013b. Recovering coseismic point ground tilts from collocated high-rate GPS and accelerometers, *Geophys. Res. Lett.,* **40**(19), 4095–4100.

Genrich, J.F. & Bock, Y., 2006. Instantaneous geodetic positioning with 10–50 Hz GPS measurements: noise characteristics and implications for monitoring networks, *J. geophys. Res.,* **111**, B03403, doi:10.1029.2005JB003617.

Haberling, S., Rothacher, M., Zhang, Y., Clinton, J.F. & Geiger, A., 2015. Assessment of high-rate GPS using a single axis shake table, *J. Geod.,* **89**(7), 697–709.

Heimlich, C., Gourmelen, N., Masson, F., Schmittbuhl, J., Kim, S.-W. & Axxola, J., 2015. Uplift around the geothermal power plant of Landau (Germany) as observed by InSAR monitoring, *Geotherm. Energy,* **3**(2), doi:10.1186/s40517-014-0024-y.

Houlié, N., Briole, P., Bonforte, A. & Puglisi, G., 2006. Large scale ground deformation of Etna observed by GPS between 1994 and 2001, *Geophys. Res. Lett.,* **33**, doi:10.1029/2005GL024414.

Houlié, N., Dreger, D. & Kim, A., 2014. GPS source solution of the 2004 Parkfield earthquake, *Sci. Rep.,* **4**, 3646, doi:10.1038/srep03646.

Houlié, N., Occhipinti, G., Blanchard, T., Shapiro, N., Lognonné, P. & Murakami, M., 2011. New approach to detect seismic surface waves in 1 Hz-sampled GPS time series, *Sci. Rep.,* **1**(44), doi:10.1038/srep00044.

Houlié, N., Woessner, J., Giardini, D. & Rothacher, M., 2018. Lithosphere strain rate and stress field orientations across the Alpine arc in Switzerland, accepted, *Sci. Rep.,* doi:10.1038/s41598-018-20253-z.

Jokinen, A., Feng, S., Schuster, W., Ochieng, W., Hide, C., Moore, T. & Hill, C., 2013. Integrity monitoring of fixed ambiguity Precise Point Positioning (PPP) solutions, *Geo-spatial Inf. Sci.,* **16**(3), 141–148.

Kaloop, M.R. & Hu, J.W., 2015. Optimizing the de-noise neural network model for GPS time-series monitoring of structures, *Sensors,* **15**(9), 24428–24444.

Kawamoto, S., Hiyama, Y., Ohta, Y. & Mishimura, T., 2016. First result from the GEONET real-time analysis system (REGARD): the case of the 2016 Kunamoto earthquakes, *Earth Plantes Space,* **68**(1), 190, doi:10.1186/s40623-016-0564-4.

Kawamoto, S., Ohta, Y., Hiyama, Y., Todoriki, M., Nishimura, T., Furuya, T., Sato, Y., Yahagi, T. & Miyagawa, K., 2017. REGARD: a new GNSS-based real-time finite fault modeling system for GEONET, *J. geophys. Res.: Solid Earth,* **122**, 1324–1349.

Kelevitz, K., Houlié, N., Giardini, D. & Rothacher, M., 2017. Performance of high-rate GPS waveforms at long periods: moment tensor inversion of the 2003 M8.3 Tokachi-Oki earthquake, *Bull. seism. Soc. Am.,* doi:10.1785/0120160338.

Koketsu, K. *et al.*, 2011. A unified source model for the 2011 Tohoku earthquake, *Earth planet. Sci. Lett.,* **310**, 480–487.

Kristensen, L. & Blikra, L.H., 2011. Monitoring displacement of the Mannen rockslide in Western Norway, in *Proc. 2nd World Landslide Forum*, Rome, Italy.

Larson, J.M., Bodin, P. & Gomberg, J., 2003. Using 1-Hz GPS data to measure deformation caused by the Denali Fault Earthquake, *Science,* **300**, 1421–1424.

Larson, K.M., 2013. A new way to detect volcanic plumes, *Geophys. Res. Lett.,* **40**(11), 2657–2660.

Lewis, M.A. & Ben-Zion, Y., 2008. Examination of scaling between earthquake magnitude and proposed early signals in *P* waveforms from very near source stations in a South African gold mine, *J. geophys. Res.,* **113**, B09305, doi:10.1029/2007JB005506.

Lienhart, W., 2015. Case studies of high-sensitivity monitoring of natural and engineered slopes, *J. Rock Mech. Geotech. Eng.,* **7**, 379–384.

Li, X., Zhang, X. & Ge, M., 2011. Regional reference network for augmented precise point positioning for instantaneous ambiguity resolution, *J. Geod.*, **85**(3), 151–158

Llubes, M. *et al.*, 2008. Multi-technique monitoring of ocean tide loading in northern France, *C. R. Geosci.,* **340**, 379–389.

Maercklin, N., Festa, G., Colombelli, S. & Zollo, A., 2012. Twin ruptures grew to build up the giant 2011 Tohoku, Japan, earthquake, *Sci. Rep.,* **709**(2), 1–7.

Mao, A., Harrison, C.G.A. & Dixon, H.A., 1999. Noise in GPS time series, *J. geophys. Res.,* **104**(B2), 2797–2816.

Melgar, D., Crowell, B., Bock, Y. & Haase, J., 2013. Rapid modeling of the 2011 Mw 9.0 Tohoku-oki earthquake with seismogeodesy, *Geophys. Res. Lett.,* **40**, 2963–2968.

Mertikas, S.P. & Damianidis, K.I., 2007. Monitoring the quality of GPS station coordinates in real time, *GPS Solut.,* **11**, 119–128.

Michel, C., Kelevitz, K., Houlié, N., Edwards, B., Psimoulis, P., Su, Z., Clinton, J. & Giardini, D., 2017. The potential of high-rate GPS for strong ground motion assessment, *Bull. seism. Soc. Am.,* **107**(3), doi:10.1785/0120160296.

Michoud, C., Bazin, S., Blikra, L.H., Derron, M.-H. & Jaboyedoff, M., 2013. Experiences from site-specific landslide early warning systems, *Nat. Hazards Earth Syst. Sci.,* **13**, 2659–2673.

Moschas, F., Avallone, A., Saltogianni, V. & Stiros, S.C., 2014. Strong motion displacement waveforms using 10-Hz precise point positioning GPS: an assessment based on free oscillation experiments, *Earthq. Eng. Struct. Dyn.,* **43**(12), 1853–1866.

Moschas, F. & Stiros, S., 2013. Noise characteristics of high-frequency, short-duration GPS records from analysis of identical, collocated instruments, *Measurement,* **46**(4), 1488–1506

Msaewe, H.A., Hancock, C.M., Psimoulis, P.A., Roberts, G.W., Bonenberg, L. & de Ligt, H., 2017. Investigating multi-GNSS performance in the UK and China based on zero-baseline measurement approach, *Measurement,* **102**, 186–199.

Newman, A.V. *et al.*, 2012. Recent geodetic unrest at Santorini Caldera, Greece, *Geophys. Res. Lett.,* **39**(6), L06309, doi:10.1029/2012GL051286.

Ohta, Y., Meiano, I., Sagiya, T., Kimata, F. & Hirahara, K., 2006. Large surface wave of the 2004 Sumatra-Andaman earthquake captured by the very long baseline kinematic analysis of 1-Hz GPS data, *Earth Planets Space,* **58**, 153–157.

Ohta, Y. *et al.*, 2012. Quasi real-time fault model estimation for near-field tsunami forecasting based on RTK-GPS analysis: application to the 2011 Tohoku-Oki earthquake (M_W9.0), *J. geophys. Res.,* **117**, B02311, doi: 10.1029/2011JB008750.

Olson, E.L. & Allen, R.M., 2005. The deterministic nature of earthquake rupture, *Nature,* **438**, 212–215.

Peppa, I., Psimoulis, P. & Meng, X. 2018. Using the signal-to-noise ratio of GPS records to detect motion of structures, *Struct. Control Health Monit.,* **25**(2), e2080, doi:10.1002/stc.2080.

Plag, H.-P., Blewitt, G. & Bar-Sever, Y., 2012. Rapid determination of earthquake magnitude and displacement field from GPS-observed coseismic offsets for tsunami warning, 1182–1185, in *2012 IEEE International Geoscience and Remote Sensing Symposium (IGARSS)*, Munich, Germany.

Poggi, V., Edwards, B. & Fah, D., 2013. Reference S-wave velocity profile and attenuation models for ground motion prediction equations: Application to Japan, *Bull. Seism. Soc. Am.,* **103**, 2645–2656.

Psimoulis, P, Houlié, N., Meindl, M. & Rothacher, M., 2014. Long-period surface motion of the multipatch M_w9.0 Tohoku-Oki earthquake, *Geophys. J. Inter.,* **199**, 968–980.

Psimoulis, P., Houlié, N. & Behr, Y., 2018. Real-time magnitude characterization of large earthquakes using the predominant period derived from 1 Hz GPS data, *Geophys. Res. Lett.,* **45**(2), 517–526

Psimoulis, P., Houlié, N., Meindl, M. & Rothacher, M., 2015. Consistency of PPP GPS and strong-motion records: case study of M_w9.0 Tohoku-Oki 2011 earthquake, *Smart Struct. Syst.,* **16**(2), 347–366.

Psimoulis, P., Pytharouli, S., Karabalis, D. & Stiros, S., 2008. Potential of Global Positioning System (GPS) to measure frequencies of oscillations of engineering structures, *J. Sound Vib.,* **318**(3), 606–623

Psimoulis, P. & Stiros, S., 2012. A supervised learning computer-based algorithm to derive the algorithm of oscillations of structures using noisy GPS and Robotic Theodolites (RTS) records, *Comput. Struct.,* **92–93**, 337–348.

Sagiya, T., 2004. A decade of GEONET: 1994–2003—the continuous GPS observation in Japan and its impact on earthquake studies, *Earth Planets Space,* **56**, xxix–xli.

Saleh, B., Blum, P.A. & Delorme, H., 1991. New silica compact tiltmeter for deformations measurement, *J. Surv. Eng.,* **117**, 27–35.

Shearer, P.M., 1999. *Introduction to Seismology,* Cambridge Univ. Press.

Suzuki, W., Aoi, S., Sekiguchi, H. & Kunugi, T., 2011. Rupture process of the 2011 Tohoku-Oki megathrust earthquake (M9.0) inverted from strong-motion data, *Geophys. Res. Lett.,* **38**, L00G16.

Teferle, N., William, S.D.P., Kierulf, H.P., Bingley, R.M. & Plag, H.P., 2008. A continuous GPS coordinate time series analysis strategy for high-accuracy vertical land movements, *Phys. Chem. Earth,* **33**(3–4), 205–216.

Trota, A., Houlié, N., Briole, P., Gaspar, J.L. & Sigmundsson, F., 2006. Deformations of the Furnas and Sete Cidade Volcanoes. Velocities and further investigations, *Geophys. J. Int.,* **166**, 952–956.

Tu, R., Wang, R., Ge, M., Walter, T.R., Ramatschi, M., Milkereit, C., Bindi, D. & Dahm, T. 2013. Cost-effective monitoring of ground motion related to earthquakes, landslides, or volcanic activity by joint use of a single-frequency GPS and a MEMS accelerometer, *Geophys. Res. Lett.,* **40**, 3825–3829.

Wang, G., Phillips, D., Joyce, J. & Rivera, F.O., 2011. The integration of TLS and continuous GPS to study landslide deformation: a case study in Puerto Rico, *J. Geod. Sci.,* **1**(3), 25–34.

Wang, G.-Q. 2012. Kinematics of the Cerca del Cielo, Puerto Rico landslide derived from GPS observations, *Landslides,* **9**, 117–130.

Williams, S.D.P., Bock, Y., Fang, P., Jamason, P., Nikolaidis, R.M., Prawirodirdjo, L., Miller, M. & Johnson, D.J. 2004. Error analysis of continuous GPS position time series, *J. geophys. Res.,* **109**(3), B03412 1–19.

Wright, T., Houlié, N., Hildyard, M. & Iwabuchi, T., 2012. Real-time, reliable magnitude for large earthquakes from 1 Hz GPS precise point positioning: The 2011 Tohoku-Oki (Japan) earthquake, *Geophys. Res. Lett.,* **39**, L12302.

Wu, H., Li, K., Shi, W., Clarke, K.C., Zhang, J. & Li, H., 2015. A wavelet hybrid approach to remove the flicker noise and the white noise from GPS coordinate time series, *GPS Solut.,* **19**(4), 511–523.

Ying, L., Wu, X., Lin, C. & Jiang, L., 2014. Traumatic severity and trait resilience as predictors of posttraumatic stress disorder and depressive symptoms among adolescent survivors of the Wenchuan earthquake, *PLOS One,* **9**, e89401.

Yokota, Y.K., Koketsu, K., Hikima,, K. & Miyazaki, S., 2009. Ability of 1-Hz GPS data to infer the source process of a medium-sized earthquake: The case of the 2008 Iwate-Miyagi Nairiku, Japan, earthquake, *Geophys. Res. Lett.,* **36**, L12301.

Zhou, C., Yin, K., Cao, Y., Ahmed, B. & Fu, X., 2018. A novel method for landslide displacement prediction by integrating advanced computational intelligence algorithms, *Sci. Rep.,* **8,** 7287, doi:10.1038/s41598-018-25567-6.

SUPPORTING INFORMATION

Supplementary data are available at *GJI* online.

Figure SA1. Flow-diagram of the developed algorithm separated in two main parts.

Figure SA2. Top: the plot of the EW component of the displacement time-series of the GPS 0550 site and the acceleration of the MIG011 K-NET station, with (bottom) a close up to the first 20 s where the detection appears. In the acceleration time-series it is clear that the two different clusters correspond to the two ruptures. The ruptures are expressed in the displacement time-series as two different step responses.

Figure SA3. Plot of the radial displacement time history of each GPS site versus the corresponding distance from the epicentre. The green dots represent the seismic signal detection based on the GPS network data and on the developed algorithm. Negative and positive distances are considered the distances of the southern and northern stations from the epicentre, respectively.

Please note: Oxford University Press is not responsible for the content or functionality of any supporting materials supplied by the authors. Any queries (other than missing material) should be directed to the corresponding author for the paper.